





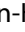











REPORT



Comprehensive engineering of a therapeutic neutralizing antibody targeting SARS-CoV-2 spike protein to neutralize escape variants

Taichi Kuramochi ^a, Siok Wan Gan ^{b*}, Adrian W.S. Ho ^b, Bei Wang ^c, Nagisa Kageji, Takeru Nambu ^{b,d}, Sayaka Iida ^{b,d}, Momoko Okuda-Miura ^b, Wei Shan Chia ^{b,e}, Chiew Ying Yeo ^{b,f}, Dan Chen ^{b,f}, Wen-Hsin Lee ^{c,g}, Eve Zi Xian Nghoh ^{c,g}, Siti Nazihah Mohd Salleh ^{c,g}, Cheng-I Wang ^{c,g}, Tomoyuki Igawa ^{h,i}, and Hideaki Shimada ^{b,j}

^aDiscovery Biologics Department, Research Division, Chugai Pharmaceutical Co., Ltd., Kamakura, Kanagawa, Japan; ^bProtein Analysis Unit, Research Division, Chugai Pharmabody Research Pte. Ltd, Singapore; ^cPharmacology Unit, Research Division, Chugai Pharmabody Research Pte. Ltd, Singapore; ^dPharmacokinetics Unit, Research Division, Chugai Pharmabody Research Pte. Ltd, Singapore; ^eProtein Production Unit, Research Division, Chugai Pharmabody Research Pte. Ltd, Singapore; ^fLead Optimization Unit, Research Division, Chugai Pharmabody Research Pte. Ltd, Singapore; ^gImmunology Network, Agency for Science, Technology and Research (A*star), Singapore; ^hDiscovery Pharmacology Department, Research Division, Chugai Pharmaceutical Co. Ltd., Kamakura, Kanagawa, Japan; ⁱTranslational Research Division, Tokyo, Japan; ^jResearch Division, Chugai Pharmabody Research Pte. Ltd., Synapse, Singapore

ABSTRACT

The emergence of escape variants of SARS-CoV-2 carrying mutations in the spike protein poses a challenge for therapeutic antibodies. Here, we show that through the comprehensive engineering of the variable region of the neutralizing monoclonal antibody 5A6, the engineered antibody, 5A6CCS1, is able to neutralize SARS-CoV-2 variants that escaped neutralization by the original 5A6 antibody. In addition to the improved affinity against variants, 5A6CCS1 was also optimized to achieve high solubility and low viscosity, enabling a high concentration formulation for subcutaneous injection. In cynomolgus monkeys, 5A6CCS1 showed a long plasma half-life and good subcutaneous bioavailability through engineering of the variable and constant region. These data demonstrate that 5A6CCS1 is a promising antibody for development against SARS-CoV-2 and highlight the importance of antibody engineering as a potential method to counteract escape variants.

ARTICLE HISTORY

Received 2 November 2021
Revised 26 January 2022
Accepted 7 February 2022

KEYWORDS

Therapeutic antibody;
antibody engineering; SARS-
CoV-2; escape variants

Introduction



The use of therapeutic antibodies to treat moderately or severely ill patients with COVID-19 has been successful at reducing viral load with a good safety profile.¹ As the spike protein of SARS-CoV-2 plays a key role in viral attachment, fusion, and entry, antibodies targeting the spike have proven to be effective in slowing and preventing viral infection.² Within the spike protein, the receptor-binding domain (RBD) mediates viral attachment to host cells expressing the angiotensin-converting enzyme 2 (ACE2) receptor. Owing to this key mechanism for viral attachment, all therapeutic antibodies currently authorized for emergency use by the US Food and Drug Administration (FDA) are directed against the RBD.³ Similarly, mRNA vaccines encoding the spike protein have been highly effective in eliciting protective antibody responses in vaccinated individuals.^{4,5}

However, an increasing number of SARS-CoV-2 variants carrying mutations within the RBD have emerged. Some of these variants contain mutations that significantly reduce neutralization by therapeutic antibodies. For example, the Beta variant (B.1.351) and Gamma variant (P.1) have become resistant to bamlanivimab and etesevimab,^{6–8} resulting in a pause by the FDA in the distribution of bamlanivimab/etesevimab as


monoclonal antibody (mAb) therapies for patients with COVID-19. Of particular concern is the Omicron variant (B.1.1.529), which was reported to escape the majority of existing therapeutic antibodies due to a large number of mutations on its RBD.⁹ Despite the emergence of escape variants, mAbs remain an important therapeutic modality for the treatment and prevention of COVID-19. There is therefore a pressing need to rapidly identify new antibodies that can effectively neutralize escape variants. Moreover, as new variants will continually emerge, the challenge presented is not so much the ability to identify new clinical antibodies, but rather the ease and speed with which this can be done.

The typical screening for new drug candidates against the escape variants requires more than one round of an extensive screening process. Large pools of diverse antibodies are progressively narrowed down using a set of criteria, such as neutralizing ability, binding affinity, and expression titer. Furthermore, the selected antibody should fit into the current cocktail therapy strategy and be compatible with another neutralizing antibody.

In contrast, the strategy of protein engineering we demonstrate here is a reverse approach of the traditional antibody selection process. Starting from a single antibody candidate,

CONTACT Taichi Kuramochi  kuramochitc@chugai-pharm.co.jp  Chugai Pharmaceutical Co. Ltd, Fuji Gotemba Research Laboratories, Komakado, Gotemba, Shizuoka, Japan.

*co-first author

 Supplemental data for this article can be accessed on the [publisher's website](#).

© 2022 The Author(s). Published with license by Taylor & Francis Group, LLC.

This is an Open Access article distributed under the terms of the Creative Commons Attribution-NonCommercial License (<http://creativecommons.org/licenses/by-nc/4.0/>), which permits unrestricted non-commercial use, distribution, and reproduction in any medium, provided the original work is properly cited.

5A6, more than 2000 variants were made by systematically mutating the complementary-determining regions (CDRs) and frameworks of the variable regions. Variants were evaluated in a battery of assays and promising substitutions were selected and combined. These mutations improved the binding affinity to the SARS-CoV-2 Spike RBD, the pharmacokinetics, and physicochemical properties while minimizing the probability of immunogenicity. The heavy chain constant region was also engineered to prolong the half-life of the antibody and ameliorate its binding to FcγR receptors.

By comprehensively engineering the antibody, we not only rescued its neutralizing efficacy against escape mutants but simultaneously optimized the antibody to attain drug-like characteristics. This methodology preserved the inherent epitope of the parent antibody while screening for the stringent physicochemical properties that are required for large-scale manufacturing and therapeutic use. By this process, 5A6 was engineered into the final candidate 5A6CCS1, which was significantly improved in terms of escape variant neutralization, physicochemical properties, and pharmacokinetics. 5A6CCS1 exhibited a long half-life in human FcRn transgenic mice and cynomolgus monkeys, and showed good manufacturability. Furthermore, it can be formulated at a high concentration for subcutaneous injection, which is better for making medical treatment more accessible during this pandemic. These data highlight how antibody engineering can be effectively used to improve existing antibody drugs so that they neutralize the emerging escape mutants, bypassing the tedious and repetitive process of re-screening for neutralizing antibodies.

Results

Antibody engineering of the anti-SARS-CoV-2 antibody

We previously reported the discovery of 5A6, as a SARS-CoV-2 neutralizing antibody that trapped the SARS-CoV-2 Spike trimer in a pre-fusion state, thereby preventing membrane fusion and syncytium formation.¹⁰ However, the antigen binding fragment (Fab) of 5A6 showed weak affinity to the RBD of the SARS-CoV-2 spike protein and exhibited modest neutralization of the SARS-CoV-2 virus.¹⁰ Most critically, 5A6 was not able to neutralize the mutant V483A pseudovirus,¹¹ raising the possibility that it may fail to neutralize other mutants as well.

Antibody engineering of 5A6 was performed with the aim to not only increase neutralization activity but also to achieve drug-like characteristics. Both the variable region and the constant region of 5A6 were engineered, taking into account multiple parameters, such as physicochemical properties, pharmacokinetics, and manufacturability. The flow of engineering is illustrated in [Figure 1a](#).

To improve the binding affinity toward the SARS-CoV-2 RBD, we comprehensively engineered the variable regions of 5A6. Each position of the CDRs and the part of framework with the potential to affect the binding affinity in the light and heavy chain were systematically substituted with the 18 other amino acids, excluding the original amino acid and cysteine. All variants were generated and evaluated in IgG1 format during the engineering process. Of the approximate 1200 mutations tested, a total of 37 single mutations across 13

positions were identified to enhance the binding affinity compared with 5A6 ([Figure 1b](#)). Before starting work on combinations, the antibodies with these 37 single mutations were assessed by size-exclusion chromatography (SEC). The mutations that showed an increase in high molecular weight species or a late column retention time, which is an indication of nonspecific binding, were excluded for combination. To further reduce the number of positions for combination, mutations that showed a marginal increment in binding affinity were deprioritized. Finally, 29 mutations were shortlisted for combination, of which 23 were from the heavy chain and 6 were from the light chain.

As it was not feasible to generate all possible combinations from the 29 mutations, we adopted a stepwise approach where combinations are incrementally introduced. This strategy is shown in [Figure 1c](#). In the first round of combination, only two mutations were combined. We selectively picked the individual mutations that conferred a large increase of affinity improvement and generated 59 double combination variants. In addition to binding affinity, the physicochemical properties of each variant were assessed by SEC, thermal shift assay (TSA), extracellular matrix (ECM) binding, affinity-capture self-interaction nanoparticle spectroscopy (AC-SINS) and hydrophobic interaction chromatography (HIC). Combination variants that showed additive or synergistic effect in binding affinity as well as acceptable physicochemical properties were shortlisted for further combinations. Conversely, combinations were discarded when there was little improvement in binding affinity or when the affinity improvement was associated with poor physicochemical behavior ([Figure 1d](#)). This process was repeated iteratively for nine cycles, with as many as 100 combination variants generated in one cycle until a final combination variant was obtained.

The frameworks of 5A6 that were obtained from the naïve human Fab phage display library were replaced with human germline frameworks, as these pose a lower immunogenicity risk than non-germline frameworks.¹⁰ The selected human germline sequences for the heavy chain of framework 1, 2, 3, and 4 were IGHV3-64*04, IGHV3-30*01, IGHV3-48*03, and JH1, respectively, and those for the light chain of framework 1, 2, 3, and 4 were IGKV1D-39*01, IGKV3-20*01, GKV1D-39*01, JK4, respectively. The replacement frameworks did not affect the binding affinity against SARS-CoV-2 RBD (data not shown).

To optimize the antibody isoelectric point (pI), we then used the final combination variant obtained from affinity maturation as a template and introduced negatively charged amino acids into the variable region at positions that did not compromise antibody binding ([Figure 1b-c](#)). This was performed in order to extend the antibody half-life of 5A6.¹² These positions were previously identified during the systematic mutagenesis of the variable region using the 18 other amino acids. After several rounds of combination for pI engineering, we selected the top 30 variants to assess their binding to mutant RBD. The final two variants were selected for further analysis. The additional assays included were pharmacokinetic assessment in human FcRn transgenic mice and cynomolgus monkeys, in vitro pseudovirus neutralization, hamster infection study,

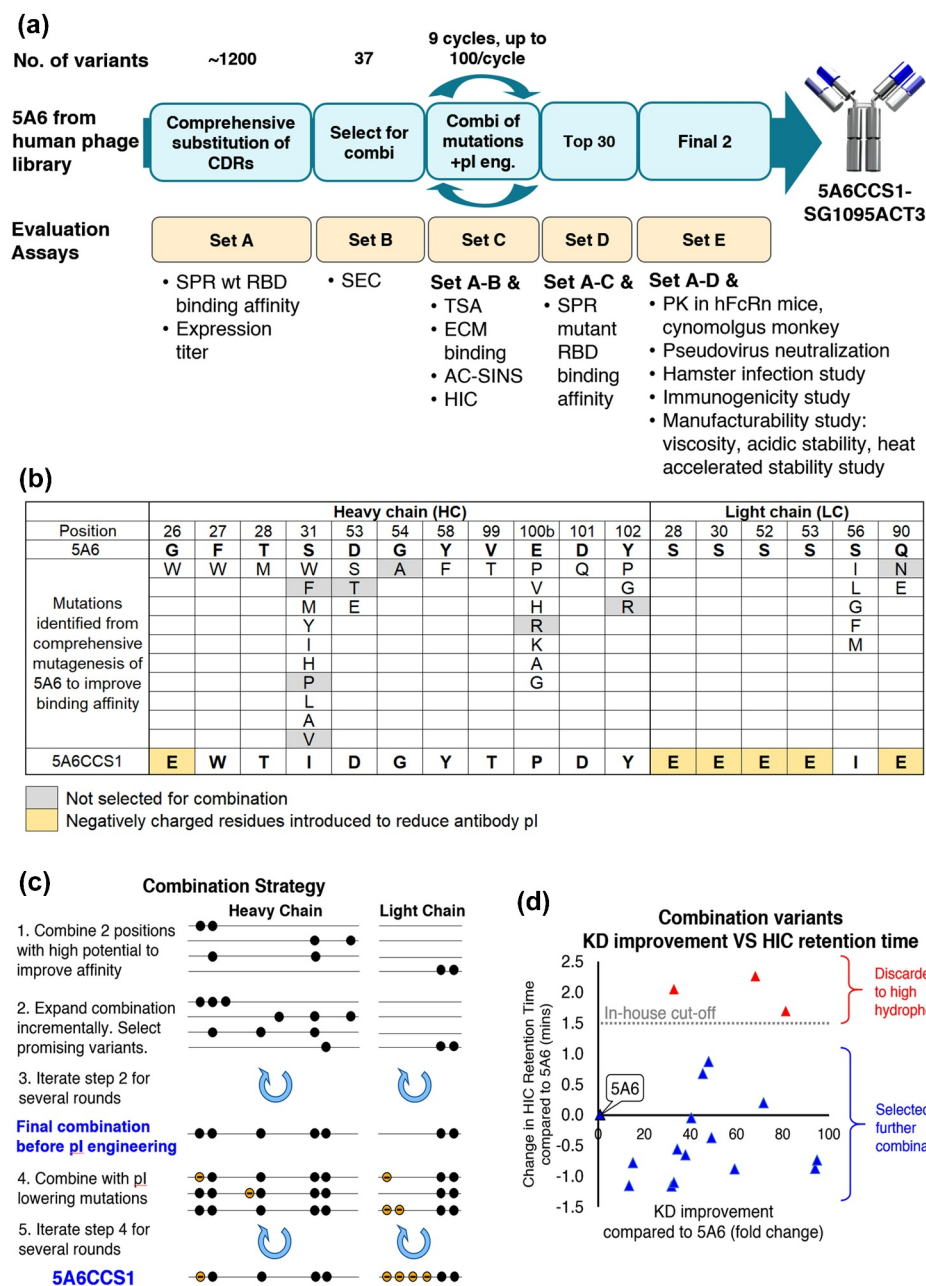


Figure 1. (a) Overview of antibody generation and engineering flow of 5A6. Diagram shows the multidimensional optimization of 5A6 to improve antigen-binding affinity, PK, and physicochemical properties. All antibodies were generated as IgG1 except for the final 2 antibodies. Evaluation of the final 2 antibodies was performed with the final Fc, SG1095ACT3. (b) List of heavy and light chain framework and CDR mutations in 5A6 identified during antibody engineering to generate 5A6CCS1. (c) Graphical illustration of the strategy employed for combination selection. Each row represents a unique antibody variant. Mutations introduced into the heavy or light chain during combination are represented by black dots. The Orange dots represent negatively charged amino acids introduced to lower the antibody pl. (d) Graph showing KD versus HIC retention time for combination variants during a particular iteration cycle. Each triangle represents one unique combination variant. Parental 5A6 marked in black is set as reference. Variants with HIC retention times exceeding the in-house cutoff mark were discarded.

immunogenicity assessment, and manufacturability assessment. For these final two variants, the heavy constant region IgG1 was replaced with SG1095ACT3, which is

a combination of mutations of our proprietary Fc technology SG1095 and ACT3. The SG1095 contains a set of mutations to reduce the binding affinity against human

Table 1. Binding affinity of 5A6 & 5A6CCS1 against RBD proteins, trimeric spike proteins, and D614G trimeric spike proteins of SARS-CoV-2.

Antibody	SARS-CoV-2 S protein RBD ^a			Trimeric SARS-CoV-2 S protein ^b			Trimeric SARS-CoV-2 S protein (D614G) ^b					
	ka (1/Ms)	kd (1/s)	KD (M)	ka (1/Ms)	kd (1/s)	KD (M)	ka (1/Ms)	kd (1/s)	KD (M)			
5A6	1.65E+06	7.01E-02	4.25E-08	1.76E+06	9.04E-04	5.13E-10	2.25E+06	7.22E-04	3.21E-10			
5A6CCS1	1.45E+06	5.72E-08	#	3.95E-14	1.57E+06	1.65E-06	#	1.05E-12	1.95E+06	2.98E-07	#	1.53E-13

[#]kinetic constant kd is approaching the limit that can be measured by the instrument.

^aAntibody was captured on a protein A/G sensor surface and different concentrations of specific antigen were injected.

^bAntigen was captured on an anti-His tag sensor surface and different concentrations of each antibody were injected. The KD values represent apparent KD.

FcγRs while maintaining C1q binding to avoid the risk of antibody-dependent enhancement of infection. The ACT3 contains a set of mutations to increase FcRn binding within acidic endosomes for a longer plasma half-life of the antibody.¹² At the end of this evaluation process, we picked the final candidate, 5A6CCS1-SG1095ACT3.

Generation of strong affinity and neutralizing ability of 5A6CCS1

Compared to the parental 5A6, 5A6CCS1 had more than 1000-fold improved binding affinity against the RBD and trimeric Spike proteins of SARS-CoV-2, as shown in Table 1. 5A6CCS1 achieved a much slower dissociation rate than 5A6, whereas the association rate was comparable between the two antibodies. The dissociation rate of 5A6CCS1 binding toward the RBD and the trimeric spike proteins of SARS-CoV-2 reached the limitation of kinetic fitting measured with the Biacore 8 K instrument under the current conditions. The binding sensorgram is shown in Supplementary Figure 1.

Next, we compared the binding of 5A6CCS1 and 5A6 against a panel of SARS-CoV-2 RBD mutants using surface plasmon resonance. These RBD mutants represent a stretch of amino acids near the binding epitope of 5A6. The panel also includes mutations seen in widely circulating variants of concern, such as the N501Y mutation in the Alpha variant and K417N in the Beta variant. As shown in Figure 2, the parental 5A6 antibody was observed to be sensitive to many mutations along the RBD, namely, N481D, G482S, V483A, E484K, E484Q, G485S, F486S, and F490S. In particular, binding to the E484K and F490S mutants was severely affected; the binding response was barely detectable under the current assay conditions. In contrast, affinity-improved 5A6CCS1 rescued the binding to these mutations, although its binding to E484K RBD was decreased by 30% compared to the wildtype (WT) RBD.

To confirm if this improved affinity can be translated to enhanced neutralization of the virus, we evaluated the neutralization potential of 5A6CCS1 against pseudoviruses expressing WT or mutant SARS-CoV-2 Spike glycoprotein tagged with

a luciferase reporter. Pseudovirus neutralization was evaluated using Chinese hamster ovary (CHO) cells stably expressing human ACE2 (CHO-ACE2). The following mutant pseudoviruses with various single amino acid mutations were generated: K417N, V483A, E484K, N501Y, and D614G. In addition, pseudoviruses for variants of concern (VOCs) (Alpha, Beta, Gamma, Delta, Omicron) and variants of interest (VOIs) (Kappa, and Epsilon) were also generated. As shown in Figure 3a, the parental 5A6 antibody was not able to neutralize the V483A and E484K single mutant pseudoviruses. Poor neutralization was also observed in Beta, Gamma, Kappa, and Omicron variants. In contrast, the affinity-improved 5A6CCS1 was able to neutralize V483A, E484K, and all the VOCs and VOIs generated for the pseudovirus neutralization assay.

We also compared the ability of 5A6CCS1 with etesevimab and bamlanivimab to neutralize the D614G and Delta variant pseudoviruses. As shown in Figure 3b, 5A6CCS1 had comparable neutralization to etesevimab and bamlanivimab against the D614G variant. For the Delta variant, 5A6CCS1 and etesevimab showed similar neutralization, whereas bamlanivimab did not exhibit any neutralizing activity.

Characterization of physicochemical properties of 5A6 antibodies

Next, we evaluated the physicochemical properties of 5A6 and 5A6CCS1 in various assays to assess its drug-likeness as the clinical candidate. As shown in Table 2, the engineered variant, 5A6CCS1 showed good physicochemical properties in SEC, AC-SINS, ECM, HIC, and TSA. In particular, 5A6CCS1 showed low aggregation tendency and achieved a main peak in SEC analysis of 98.3%, compared to 75.9% in 5A6.

To assess the ability to formulate 5A6CCS1 as a subcutaneous drug, we evaluated the developability of 5A6CCS1 at high concentration. The viscosity of 5A6CCS1 at high concentration in a formulation buffer at pH 6.0 was evaluated. 5A6CCS1 showed good solubility at a high concentration at 208 mg/mL and the viscosity reading was 21.49 mPa.s with optimal syringeability for subcutaneous administration.¹³ We conducted a heat acceleration stability study of 5A6CCS1 at 150 mg/mL in a formulation buffer

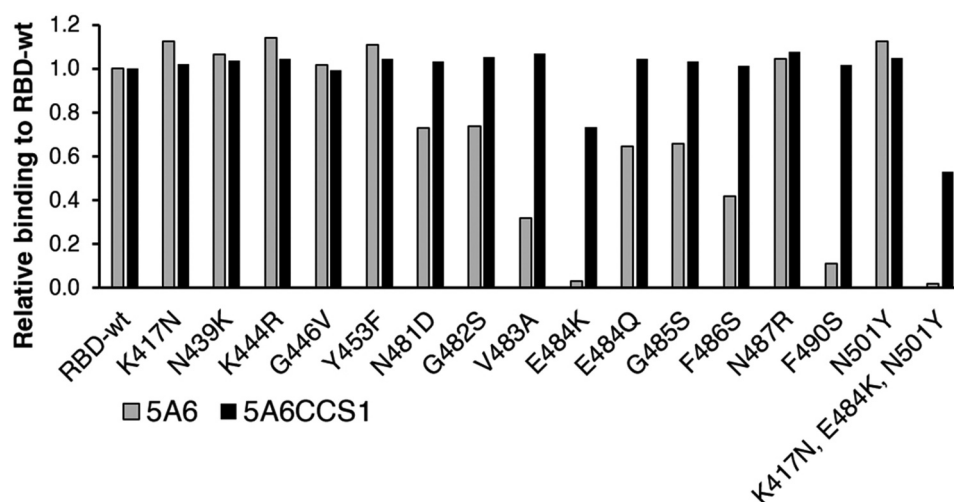


Figure 2. Biacore binding analysis of 5A6 & 5A6CC1 binding to the RBD mutants.

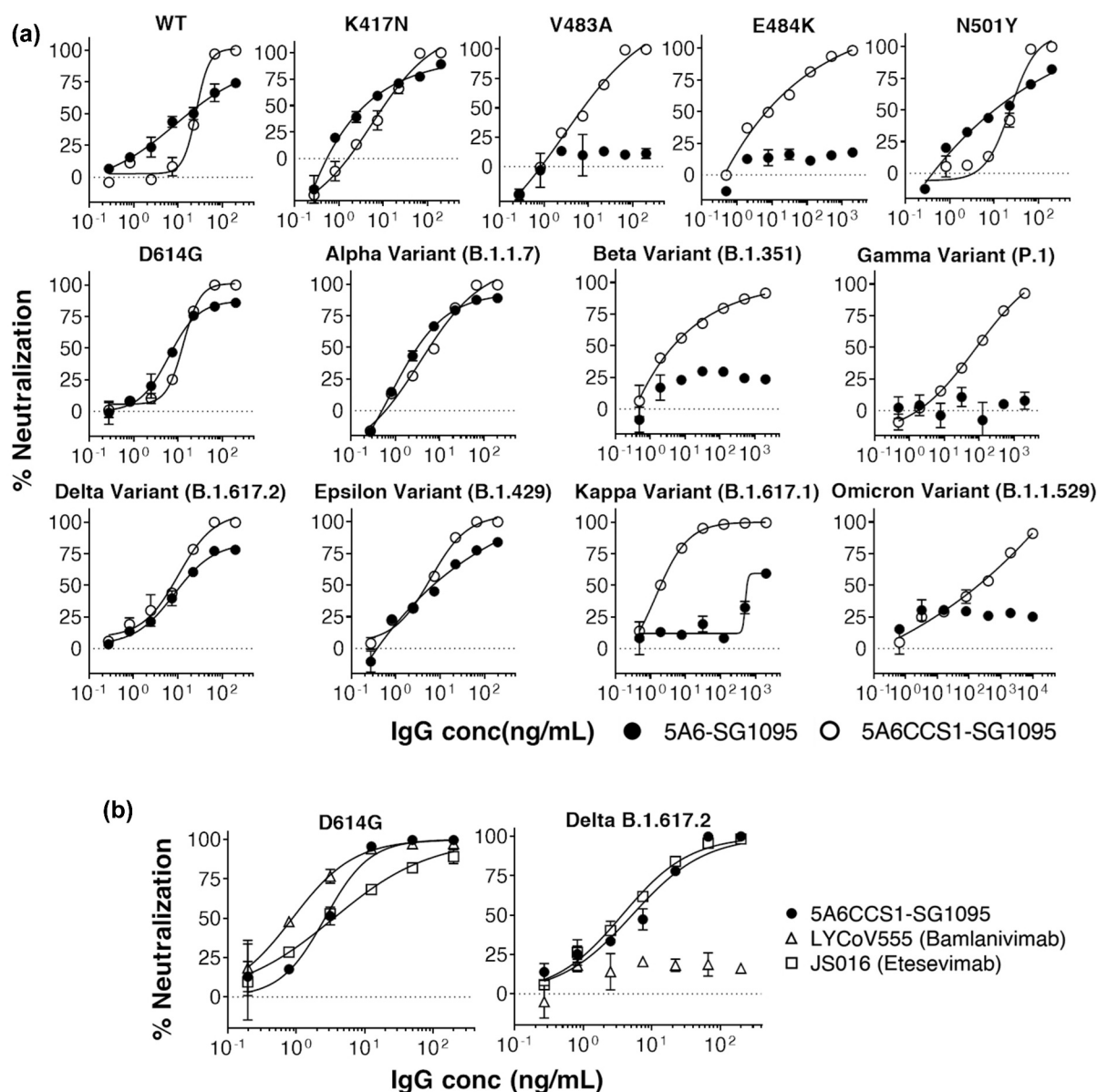


Figure 3. SARS-CoV-2 pseudovirus neutralization. (a) Infection of CHO-ACE2 cells by SARS-CoV-2 pseudovirus was evaluated in the presence of 5A6 or 5A6CCS1. (b) Comparison of 5A6CCS1 with etesevimab and bamlanivimab to neutralize the D614G and Delta variant pseudoviruses. Data are presented as mean \pm s.d from duplicate wells and are representative of two independent experiments.

Table 2. Evaluation of physicochemical properties of 5A6CCS1 Ab in SEC, AC-SINS, ECM, HIC, and TSA assays.

Ab name	SEC (main peak %)	AC-SINS (λ nm)	ECM (ratio to Actemra)	HIC (RT min)	TSA (Tm1 °C)
5A6	75.9	528.2	0.879	15.57	68.5
5A6CCS1	98.3	528.4	0.585	16.20	67.7

at pH 6.0 for 2 weeks and 4 weeks at 5 °C, 25 °C and 40 °C. There was no increment of high molecular weight (HMW) components at 150 mg/mL at all three temperatures after 4 weeks. The results of the developability assessment of 5A6CCS1 are shown in Figure 4.

In addition, we obtained an antibody titer of approximately 500 mg/L of 5A6CCS1 by transient expression in Expi293 cells. These data demonstrated that 5A6CCS1 has the requisite drug-like properties for development as a subcutaneous drug.

Pharmacokinetics of 5A6 antibodies in human FcRn transgenic mice and cynomolgus monkey

Three antibodies, 5A6-SG1095, 5A6CCS1-SG1095, and 5A6CCS1-SG1095ACT3, were injected at doses of 2 mg/kg into human FcRn transgenic mice in the presence of intravenous immune globulin (IVIG) (Figure 5). Blood samples were collected until day 28 and antibody concentration was measured. The parental 5A6-SG1095 showed fast clearance (CL). As we previously demonstrated a correlation between high antibody isoelectric point (pI) and fast antibody CL,¹⁴ the variable region of 5A6CCS1 was engineered to lower the pI. By lowering pI from 9.22 to 7.83, the clearance of antibody was improved from 15.2 mL/day/kg to 8.25 mL/day/kg.

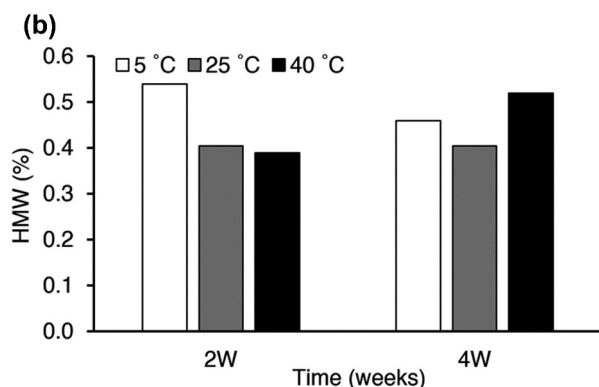
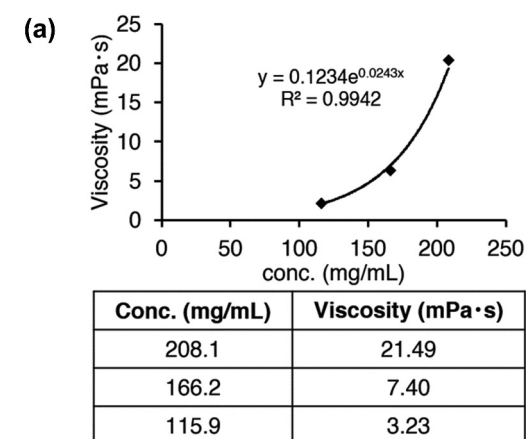


Figure 4. Developability assessment of 5A6CCS1. Viscosity measurement of 5A6CCS1 in a formulation buffer at pH 6.0 (a). HMW content analyzed by SEC for storage of 5A6CCS1 formulated at 150 mg/mL in a formulation buffer incubated at 5 °C, 25 °C, and 40 °C (b).

To further enhance the pharmacokinetics, we used the ACT3 that contains mutations to enhance the affinity toward human FcRn. The clearance of the antibody was further

reduced to 3.57 mL/day/kg. As summarized in Table 3, the clearance of 5A6CCS1-SG1095 and 5A6CCS1-SG1095ACT3 was improved by 1.8-fold and 4.3-fold, respectively, compared to 5A6-SG1095, demonstrating the effectiveness of lowering the antibody pI in combination with enhancing affinity to human FcRn.

Finally, the pharmacokinetics of 5A6CCS1-SG1095ACT3 was assessed in cynomolgus monkeys at an intravenous dose of 0.6 mg/kg and 6 mg/kg, and the antibody concentration was monitored until day 70. 5A6CCS1-SG1095ACT3 showed linear pharmacokinetics and slow clearance (Figure 6 and Table 4). The bioavailability of 5A6CCS1-SG1095ACT3 was estimated to be 99.9% when subcutaneously administered at a dose of 0.6 mg/kg.

Therapeutic efficacy of 5A6CCS1-SG1095ACT3 against SARS-CoV-2 infection

To confirm that the engineered 5A6CCS1 antibody had neutralizing potency against the live SARS-CoV-2 virus, we tested the efficacy of the antibody in a hamster model of SARS-CoV-2 infection. Hamsters were intranasally infected with 1×10^5 pfu of SARS-CoV-2 (D614G) virus, strain Slovakia/SK-BMC5/2020, and 6 hours later the 5A6CCS1 antibody was

Table 3. PK data in hFcRn transgenic mice. Area under the curve (AUC), half-life ($T_{1/2}$), and total clearance (CL) of 5A6-SG1095, 5A6CCS1-SG1095, and 5A6CCS1-SG1095ACT3 in human FcRn transgenic mice administered with IVIG after intravenous injection.

Antibody	Dosage (mg/kg)	AUC _{INF} (day*ug/mL)	CL (mL/day/kg)	$T_{1/2}$ (day)	V _{ss} (mL/day)
5A6CCS1-SG1095ACT3	2.0	564	3.57	16.7	83.4
5A6CCS1-SG1095	2.0	245	8.25	10.8	104
5A6-SG1095	2.0	136	15.2	8.24	138

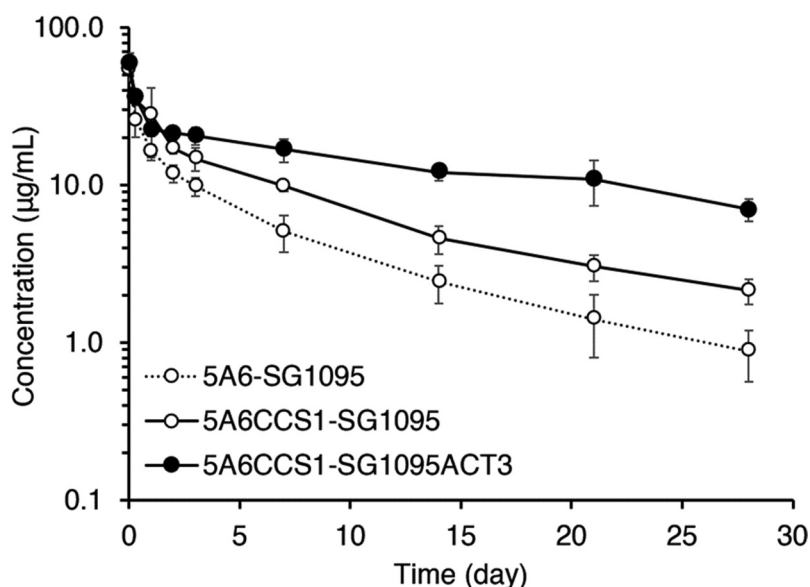


Figure 5. Pharmacokinetics of 5A6-SG1095, of 5A6CCS1-SG1095, and 5A6CCS1-SG1095 in human FcRn transgenic mice. Time profiles of plasma concentration of 5A6-SG1095, of 5A6AM1-SG1095, and 5A6CCS1-SG1095 after intravenous injection at 2 mg/mL. Each data point represents the mean \pm s.d. (n = 3).

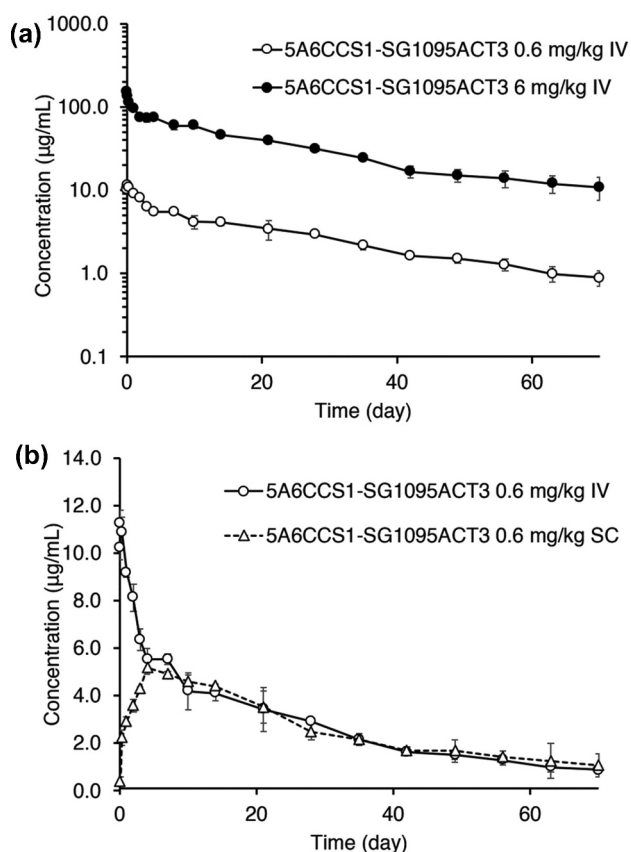


Figure 6. Pharmacokinetics of 5A6CCS1-SG1095ACT3 in cynomolgus monkeys. Time profiles of plasma concentration of 5A6CCS1-SG1095ACT3 after intravenous injection at 0.6 and 6 mg/kg (a) and intravenous or subcutaneous injection at 0.6 mg/kg (b). Each data point represents the mean \pm s.d (n = 2).

Table 4. PK data in Cynomolgus monkey. AUC, $T_{1/2}$, and CL of 5A6CCS1-SG1095ACT3 in cynomolgus monkey after intravenous or subcutaneous injection.

Dosage (mg/kg)	Dosing route	AUC _{inf} (day*ug/mL)	CL (mL/day/kg)	$T_{1/2}$ (day)	Vss or Vss/F (mL/day)	Bioavailability (%)
0.6	IV	226	2.67	25.2	92.1	NA
0.6	SC	226	2.71	28.3	107	99.9
6	IV	2918	2.10	43.4	100	NA

administered intraperitoneally. As a control antibody, IC17-hIgG1, which binds to an irrelevant antigen (KLH), was administered. The hamsters were sacrificed 4 days later, and lungs were harvested to determine the viral load. As shown in Figure 7, 5A6CCS1 significantly reduced the lung viral load as determined by qRT-PCR analysis of the SARS-CoV-2 RNA-dependent RNA polymerase gene and the ORF1ab gene.

In summary, the anti-SARS-CoV-2 Spike protein mAb, 5A6CCS1-SG1095ACT3, shows strong affinity against various SARS-CoV-2 mutant variants and successfully neutralizes virus infection. It also has excellent physicochemical properties, a long half-life, and good bioavailability. These properties enable less frequent dosage with subcutaneous injection and are expected to be effective in the prevention and treatment of COVID-19.

Discussion

We report an antibody engineering strategy to simultaneously improve virus neutralization and drug-likeness, which we demonstrated by generating a potent neutralizing IgG antibody, 5A6CCS1, against the RBD of the SARS-CoV-2 Spike. During the process of antibody engineering, it is common that mutations that improve binding inadvertently compromise the physicochemical properties of the antibody, affecting its drug-likeness and manufacturability. During the antibody engineering process of 5A6, many promising variants with potent neutralizing activities showed poor physicochemical properties, for example, precipitating during antibody purification, binding strongly to ECM, or having a high aggregation tendency (data not shown). Although assays to evaluate the physicochemical properties of antibodies have been developed, no single assay is able to assess multiple parameters, such as self-association, hydrophobicity profile, charge interaction, stability, and viscosity. Moreover, though algorithms to predict drug-like physicochemical properties have been reported,¹⁵ they are currently unable to substitute for wet lab experiments. As such, we propose that multidimensional evaluation of antibodies should be done in parallel with affinity maturation. One possible method to achieve this is by a comprehensive mutagenesis workflow, as we have described in Figure 1.

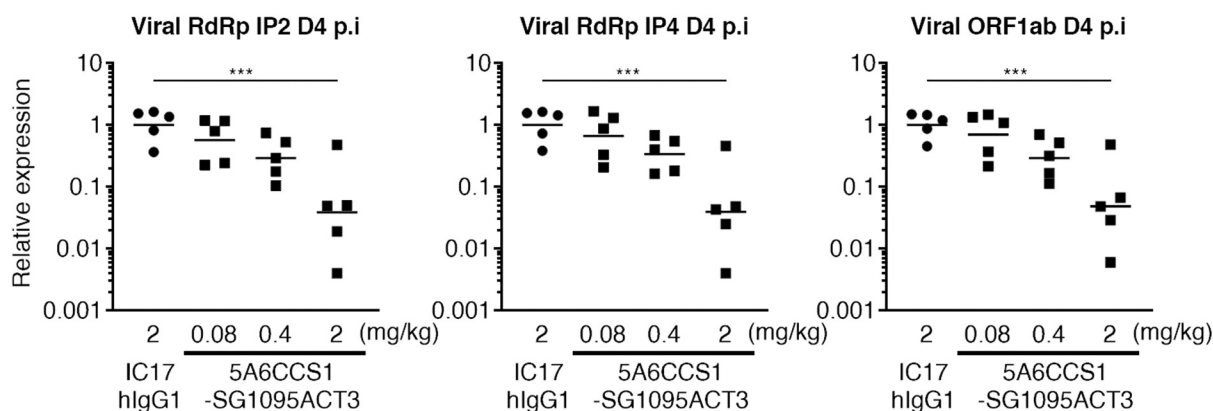


Figure 7. Therapeutic efficacy of treatment with 5A6CCS1-SG1095ACT3 in a live SARS-CoV-2 virus inoculated Hamster model. Lung viral load was determined by qPCR of the SARS-CoV-2 RNA dependent RNA polymerase (RdRp) and ORF1ab genes. Data are presented as geometric mean, n = 5 per group. *** p < .001, 1-way ANOVA with Dunnett's multiple comparison test against control group.

Results from a Phase 3 prevention trial showing that subcutaneous injection of anti-SARS-CoV-2 antibodies prevented symptomatic and asymptomatic infection of household contacts was recently reported.¹⁶ Given the pandemic setting, subcutaneous delivery of drugs is not only convenient but also important to reduce patient load on hospitals and treatment centers. 5A6CCS1 was engineered to have physicochemical properties enabling high concentration formulation for subcutaneous delivery. The small injection volume requires 5A6CCS1 to be stable and have low propensity for aggregation at higher concentration while simultaneously having a viscosity below 20 centipoise (cP) to enable the use of a pre-filled syringe or auto injector.¹³ At 208 mg/mL, 5A6CCS1 had a viscosity of 21.49 mPa.s. At 150 mg/mL, which is within a typical concentration range for subcutaneous therapeutic drugs, 5A6CCS1 showed excellent stability and solubility. The expression titer for 5A6CCS1 was approximately 500 mg/L using transient expression in Expi293 cells. As it was reported that optimizing an antibody's physicochemical properties enhances its biosynthesis in CHO cells,¹⁷ one reason for the higher yields of optimized 5A6CCS1 could be its superior biophysical properties, since we carefully selected mutations that do not affect expression titer and physicochemical properties during the engineering process.

In most antibody engineering campaigns, affinity improvement is conducted against one antigen. However, the large diversity of SARS-CoV-2 mutant RBDs presents a formidable technical challenge, as strong binding to multiple RBD mutants is required. In this study, we used the WT RBD for affinity improvement during the comprehensive mutagenesis of 5A6 CDRs. The binding affinity to mutant RBD was only evaluated at the late stages of optimization, after several rounds of iterations had been conducted. Interestingly, by improving the binding affinity to the WT RBD, significant gains in affinity were also seen in the RBD mutants tested, even toward the E484K and F490S mutations. This observation is consistent with recent reports.^{18,19} While comparing the B cells sampled from patients 1 month and 6 months after infection, Muecksch et al.¹⁸ observed that somatic mutation-mediated affinity matured SARS-CoV-2 neutralizing antibodies had neutralization potency against escape mutants. The E484K mutation in beta and gamma variants is particularly challenging because it introduces a reversal in the electrostatic charge of the side chain on top of steric clashes with antibodies. Several therapeutic antibodies have impaired binding to SARS-CoV-2 strains containing this mutation.^{7,20} Although we showed that 5A6CCS1 was able to neutralize the E484K and triple mutant, a 10-fold higher antibody concentration was required compared to the WT virus. Nonetheless, we hypothesize that re-engineering of CCS1 using the beta or gamma variant RBD can be performed to identify antibodies with improved neutralization.

As the Omicron variant emerged after this work had been submitted for possible publication, we had a unique opportunity to test in an unbiased way if the affinity engineered 5A6CCS1 indeed had broad cross-reactivity and could neutralize a newly discovered variant. Interestingly, 5A6CCS1 was able to neutralize the Omicron variant pseudovirus. Although a high dose of antibody was required for complete

neutralization, this is expected as the RBD of the Omicron variant is highly mutated. Our results thus demonstrate the utility of the antibody engineering process to create potent antibodies that are more resilient against mutations.

Antibody affinity improvement can be conducted using antibody-antigen structures derived from X-ray crystallization, nuclear magnetic resonance, or cryo-electron microscopy. Rationally designed mutations are introduced to improve the spatial interaction between the antibody and antigen. Although this targeted mutagenesis approach is effective, it is completely dependent on the availability of high-resolution structure information. The ever-growing diversity of SARS-CoV-2 mutants presents a logistical challenge for structure-based engineering. Library-based approaches such as phage or ribosome display techniques are also commonly used to conduct affinity maturation.²¹ Although hits with significant improvement in affinity can be efficiently identified, a major drawback is that these hits typically contain multiple mutations. As each mutation's effect on binding affinity and physicochemistry is not known, it is difficult to rationally combine mutations among the hits for further optimization. In contrast, a systematic and comprehensive position-by-position mutation provides a large panel of data to efficiently identify the best combination of mutations to achieve drug-likeness.

In summary, we have demonstrated that antibody engineering is a potential method to counteract escape variants and generate drug-like candidates. Antibody engineering permits multiple properties to be simultaneously evaluated and optimized in a systemic approach, therefore potentially speeding up the process of drug candidate screening. The application of this antibody engineering method goes beyond SARS-CoV-2 and can be broadly applied to any target, creating the possibility for faster and more efficient drug development programs.

Materials and methods

Antibody generation

The polynucleotides encoding variable regions of the heavy and light chain were synthesized by GenScript Inc. and were cloned into expression vectors containing a polynucleotide encoding the heavy chain constant region or the light chain constant region sequence, respectively. Recombinant antibodies were expressed transiently using the Expi293 Expression System (Thermo Fisher) according to the manufacturer's instructions. For high throughput antibody generation during the antibody engineering process, antibodies in normal IgG1 format were purified with protein A (GE Healthcare) from supernatant of transient expression. An additional purification step was performed to further evaluate the top two selected candidates by using SEC to remove HMW and low molecular weight components. The heavy chain constant region for the top two selected candidates was replaced with SG1095ACT3. The purified antibodies were kept in a formulation containing 20 mM His, 150 mM Arg, 162.1 mM Asp, 20 mM Met, pH6.0.

Antibody sequences for LY-CoV555 and JS-016, were obtained from the International Immunogenetics Information System (www.imgt.org) with seq IDs INN11876

and INN11873, respectively. Recombinant antibodies were expressed transiently using the Expi293 Expression System (Thermo Fisher) according to the manufacturer's instructions.

Biacore binding assays

The binding affinities of clone 5A6 and 5A6CCS1 toward recombinant SARS-CoV-2 S protein RBD were measured using Biacore 8 K instrument (GE Healthcare). Antibodies in IgG1 format were captured onto the Protein A/G that was immobilized onto a CM4 sensor chip using amine coupling kit (GE Healthcare). Recombinant SARS-CoV-2 S protein WT-RBD (Acrobiosystems, #SPD-C52H3) were injected at different concentrations (6.25 nM – 100 nM, two-fold serial dilution). All antibodies and analytes were prepared in ACES pH 7.4 containing 20 mM ACES, 150 mM NaCl, 0.05% Tween 20, 0.005% NaN₃. Assay temperature was set at 37 °C. Sensor surface was regenerated each cycle with 10 mM Glycine-HCl, pH 1.5. Binding affinities were determined by processing and fitting the data to 1:1 binding model using Biacore Insight Evaluation Software, version 3.0.12.15655 (GE Healthcare).

Binding activities of 5A6 and 5A6CCS1 toward a list of RBD mutants were measured with similar assay conditions. K417N (SinoBiological, #40592-V08H59), N439K (SinoBiological, #40592-V08H14), K444R (SinoBiological, #40592-V08H54), G446V (SinoBiological, #40592-V08H51), Y453F (SinoBiological, #40592-V08H80), N481D (SinoBiological, #40592-V08H70), G482S (SinoBiological, #40592-V08H53), V483A (Acrobiosystems, #SPD-C52H5), E484K (Acrobiosystems, #SRD-C52H3), E484Q (SinoBiological, #40592-v08h81), G485S (SinoBiological, #40592-V08H52), F486S (SinoBiological, 40592-V08H74), N487R (SinoBiological, #40592-V08H75), F490S (SinoBiological, 40592-V08H41), N501 (SinoBiological, #40592-V08H82), and triple RBD mutation K417N, E484K, N501Y (Acrobiosystems, #SPD-C52Hp). Recombinant SARS-CoV-2 S protein WT-RBD and mutants were injected at 100 nM concentrations. Binding response of 5A6 and 5A6CCS1 to recombinant RBD WT or mutants were normalized to capture level. Analysis of relative binding of RBD mutants to RBD WT was analyzed as binding activities of 5A6 and 5A6CCS1 toward the RBD mutants.

The binding affinities of 5A6 and 5A6CCS1 in IgG1 format binding to trimeric SARS-CoV-2 S protein were determined at 37 °C using Biacore T200 instrument (GE Healthcare). Anti-histidine antibody (GE Healthcare) was immobilized onto all flow cells of a CM5 sensor chip using amine coupling kit (GE Healthcare). Trimeric SARS-CoV-2 S protein (D614G) with a polyhistidine tag at the C-terminus (Acrobiosystems, #SPN-C52H3) and trimeric SARS-CoV-2 S protein with a polyhistidine tag at the C-terminus (Acrobiosystems, # SPN-C52H8) was captured onto the anti-histidine sensor surfaces. Then, clone 5A6 and 5A6CCS1 were injected at different concentration (6.25 nM – 100 nM, two-fold serial dilution). All antibodies and analytes were prepared in ACES pH 7.4 containing 20 mM ACES, 150 mM NaCl, 0.05% Tween 20, 0.005% NaN₃. The sensor surface was regenerated each cycle with 10 mM Gly-HCl pH 1.5. Binding kinetics and affinity were

determined by processing and fitting the data to 1:1 binding model using Biacore T200 Evaluation software, version 2.0 (GE Healthcare).

Antibody neutralization assay with SARS-CoV-2 spike glycoprotein pseudovirus

To evaluate the neutralization potential of antibodies, pseudoviruses expressing WT or mutant SARS-CoV-2 spike glycoprotein tagged with a luciferase reporter were generated. Neutralization of pseudovirus was evaluated using CHO cells stably expressing human ACE2 (CHO-ACE2, a kind gift from Professor Yee-Joo Tan, Department of Microbiology, NUS & IMCB, A*STAR, Singapore).²² Pseudotyped viral particles expressing SARS-CoV-2 Spike protein were produced as in our previous study.¹⁰ Briefly, 30 million 293 T cells were transfected with 12 µg pMDLg/pRRE (a gift from Didier Trono, Addgene #12251), 6 µg pRSV-Rev (a gift from Didier Trono, Addgene #12253), 24 µg pHIV-Luc-ZsGreen (a gift from Bryan Welm, Addgene #39196) and 12 µg pTT5LnX-CoV-SP (expressing SARS-CoV-2 Spike protein, GenBank: YP_009724390.1, a kind gift from DSO National Laboratories) using Lipofectamine 2000 transfection reagent (Invitrogen, Cat#11668-019). The transfected cells were cultured in a 37°C incubator for 3 days. Viral supernatant was harvested, centrifuged, and filtered through a 0.45 µm filter unit (Sartorius, Cat#16555). Lenti-X p24 rapid titer kit (Takara Bio, Cat#632200) was used to quantify the viral titers. pTT5LnX-CoV-SP plasmids with different mutations were generated using QuickChange Lightning Multi Site-Directed Mutagenesis Kit (Agilent, Cat#210513) and were used to generate mutant pseudoviruses. CHO-ACE2 cells were seeded at a density of 3.2×10^4 cells in 100 µL of complete medium without Geneticin in 96-well Flat Clear Bottom Black Polystyrene TC-treated Microplates (Corning, #3904). Serially diluted IgGs were incubated in a 96-well flat-bottom cell culture plate (Costar, #3596) with an equal volume of pseudovirus (6 ng of p24) at the final volume of 50 µL at 37 °C for one hour, and the mixture was added to the monolayer of pre-seeded CHO ACE2 cells in duplicate. After one hour of pseudovirus infection at 37 °C, 150 µL of culture medium was added to each well and the cells were further incubated for another 48 hours. Upon removal of culture medium, cells were washed with sterile phosphate-buffered saline, and then lysed in 20 µL of 1x Passive lysis buffer (Promega, E1941) with gentle shaking at 400 rpm at 37 °C for 30 minutes. Luciferase activity was then assessed using the Luciferase Assay System (Promega, E1510) on a Promega GloMax Luminometer. The relative luciferase units (RLU) were converted to percent neutralization and plotted with a non-linear regression curve fit using PRISM (Graphpad).

Pseudoviruses for VOCs and VOIs were also generated with multiple mutations on the S gene: Alpha (del69-70/del144-145/N501Y/A570D/D614G/P681H/T716I/S982A/D1118H), Beta (D80A/del242-245/R246I/K417N/E484K/N501Y/D614G/A701V), Gamma (L18F/T20N/P26S/D138Y/R190S/K417T/E484K/N501Y/D614G/H655Y/T1027I/V1176F), Delta (T19R/

G142D/E156G/del157-158/L452R/T478K/D614G/P681R/D950N), Kappa (T95I/E154K/L452R/E484Q/D614G/P681R), Epsilon (S13I/W152G/L452R/D614G), and Omicron (A67V/del69-70/T95I/G142D/del143-145/del211/L212I/ins214EPE/G339D/S371L/S373P/S375F/K417N/N440K/ G446S/S477N/T478K/E484A/Q493R/G496S/Q498R/N501Y/Y505H/T547K/D614G/H655Y/N679K/P681H/ N764K/D796Y/N856K/Q954H/N969K/L981F).

PK study using human FcRn transgenic mice

Antibodies were intravenously administered at 2 mg/kg into 6-weeks old male human FcRn transgenic mice (B6.mFcRn2/2.hFcRn Tg line 32+/+ mouse, Jackson Laboratories) with a single intravenous injection at 1 g/kg of hIgG (Hizentra, CSL Behring) to mimic endogenous human IgGs. Blood samples were collected at 5 min, 7 hr, 1, 2, 3, 7, 14, 21, and 28 days after administration. The plasma antibody concentration was determined using coating Multi-Array 96-well plate (Meso Scale Discovery) with SARS-CoV-2 S Protein RBD, His Tag (Acro Biosystems), and detected with SULFO-TAG labeled anti-delta-GK antibody (in-house).

PK study using cynomolgus monkey

Antibodies were intravenously or subcutaneously administered at 0.6 or 6 mg/kg into 3–5 years old male cynomolgus monkeys. Blood samples were collected at 2, 7 hours, 1, 2, 3, 4, 7, 10, 14, 21, 28, 35, 42, 49, 56, 63, and 70 days after administration. For animals that received intravenously administered antibodies, blood samples were additionally collected at 5 min after administration. The plasma antibody concentration was determined using coating 384-well High Bind plate (Meso Scale Discovery) with Goat anti-Human IgG (Southern Biotech, #2049-01), and detected with Goat anti-Human Kappa Light Chain biotin (Immuno-Biological Laboratories, #17249) and SULFO-TAG Labeled Streptavidin (Meso Scale Discovery, #R32AD).

Antibody treatment of golden syrian hamsters infected with SARS-CoV-2

Female Golden Syrian Hamsters (Janvier labs, France), 6–8 weeks old, were weighed and allocated into seven homogeneous groups of five animals for each study. Hamsters were anesthetized using isoflurane and infected intranasally with 70 μ L of virus suspension containing 1×10^5 pfu of SARS-CoV-2 (D614G) virus, strain Slovakia/SK-BMC5/2020 (European Virus Archive global). Six hours after infection, hamsters received an intraperitoneal injection of antibodies at the indicated dose. Hamsters were sacrificed 4 days after infection. Hamsters were anesthetized using a cocktail of Zoletil (30 mg/kg) and Xylazine (10 mg/kg) injected intraperitoneally, followed by gentle cervical dislocation, thoracotomy, and terminal blood sampling. The left lungs were placed in RNAlater overnight at 4 °C then stored at –80 °C until RNA extraction for quantification of viral load by qRT-PCR.

Virus load detection by qPCR

Viral load determination in lungs by qRT-PCR Extraction of viral RNA was performed using QIAamp viral RNA mini kit (Qiagen), and RT-PCR was performed using SuperScript III One-Step qRT-PCR Kit1 (Life Technologies, #11732). SARS-CoV-2 RNA was quantitated using IP2 and IP4 primers that detect the RNA-dependent RNA polymerase gene (RdRp) and ORF1ab gene detection primers.

RdRp gene IP2 primers: IP2-12669Fw 5'-ATGAGCTTAGT CCTGTTG, IP2-12759Rv 5'-CTCCCTTTGTTGTGTTGT. IP2 probe sequence: IP2-12696bProbe(+) AGATGTCTTGTGCT GCCGGTA [5'] Hex [3'] BHQ-1. RdRp gene IP4 primers: IP4-14059Fw 5'-GGTAACTGGTATGATTTCCG, IP4-14146Rv5' -CTGGTCAAGGTTAATATAGG. IP4 probe sequence: IP4-14084Probe(+) TCATACAAACCACGCCAGG [5'] Fam [3'] BHQ-1. ORF1ab_Fw 5'-CCGCAAGGTTCTTCTTCGTAAG, ORF1ab_Rv 5'-TGCTATGTTTAGTGTTCCAGTTTTC. ORF1ab probe sequence: AAGGATCAGTGCCAAGCTCG TCGCC [5'] Hex [3'] BHQ-1.

Statistical analysis

Statistical analysis was performed using PRISM (Graphpad).

Heat accelerated stability study

Samples were concentrated to 150 mg/mL using the Amicon Ultra 4 mL 30 K (Millipore #UFC803024) in a formulation buffer (20 mM His, 150 mM Arg, 162.1 mM Asp, 20 mM Met, pH6.0). Samples were kept at three temperatures: 5 °C, 25 °C, and 40 °C. Time points were taken at day 14, and 28. Samples were then analyzed by SEC (Tosoh Bioscience #A00166) with running buffer containing 50 mM sodium phosphate, 300 mM sodium chloride, pH 7.0.

Viscosity measurement

Samples were concentrated to around 200 mg/mL using the Amicon Ultra 4 mL 30 K (Millipore #UFC803024) in a formulation buffer (20 mM His, 150 mM Arg, 162.1 mM Asp, 20 mM Met, pH6.0). The viscosity of mAb solutions was measured at 25 °C by an electromagnetic spinning (EMS) method using an EMS viscometer (Kyoto Electronics Manufacturing, Kyoto, Japan). An aluminum ball was put in a glass vial containing the samples and the viscosity of each sample solution was obtained at rotation speeds at 1000 rpm. The viscosity of the liquid sample can be calculated from the rotational speed of the aluminum ball measured by using the flash lamp and the CCD video camera.

Affinity-capture self-interaction nanoparticle spectroscopy

In AC-SINS assay, 0.1 mg/mL concentration of the test antibodies were added to gold nanoparticles (Ted Pella Inc. #15705) pre-coated with 80% of polyclonal goat anti-human IgG Fc (Jackson ImmunoResearch #109-005-098) as capturing and 20% of goat nonspecific antibody (Jackson ImmunoResearch

#005-000-003). Test antibodies were incubated with the pre-coated gold nanoparticles for 2 hours at room temperature and the wavelength shift was measured using SpectraMax M2 (Molecular Devices).

Size exclusion chromatography

Test antibodies were injected to ACQUITY UPLC Protein BEH200, 1.7 μ m, 4.6 mm \times 150 mm column (Waters) with a linear gradient of mobile phase A (50 mM Phosphate, 300 mM NaCl, pH7.0) over 10 min at a flow rate of 0.3 mL/min with UV absorbance monitoring at 280 nm and 220 nm. Temperature for column compartment was set at 30 °C.

Hydrophobic interaction chromatography

Test antibodies were injected to TSKgel Ether-5PW 7.5 \times 75 mm (TOSOH), connected to the Acquity HPLC (Waters). The column was equilibrated with 90% mobile phase A (20 mM Na-phosphate, 1.5 M (NH₄)₂SO₄, pH7.0) and 10% mobile phase B (20 mM Na-phosphate, pH7.0). The samples were eluted using an inverted gradient from mobile phase A to mobile phase B over 23 min at a flow rate of 0.7 mL/min with UV absorbance monitoring at 280 nm. Temperature for column compartment was set at 25 °C.

Thermal shift assay

The T_m was determined using a Rotor-gene Q-5PLEX (QIAGEN). Briefly, 18 μ L of 0.1 mg/mL sample was mixed with 2 μ L of 100 \times SYPRO orange (Invitrogen, #S6651). The plate was ramped from 30 °C to 99 °C with 0.4 °C/step, and the temperature was held for 90s for the first step and 6s for subsequent step. The T_m was assigned using the first derivative of the raw data from the Rotor-Gene Q Software 2.3.5.1. In high throughput screening, the first peak of the melting curve (T_{m1}) was referenced for ranking among antibody variants.

Extracellular matrix binding assay

The binding to ECM was measured using electrochemiluminescence assay. BD Matrigel Basement Membrane Matrix (BD) was dispensed onto a MULTI-ARRAY 96-well Plate (Meso Scale Discovery) and incubated overnight at 4 °C. SULFO-Tag labeled goat anti-human antibody (Meso Scale Discovery, #R32AJ) was used as detection antibody. 3 μ g/mL concentration of test antibodies diluted with ACES buffer pH 7.4 (20 mM ACES, 150 mM NaCl, 1.2 mM CaCl₂, 0.01% Tween 20, and 0.1% bovine serum albumin) were dispensed onto ECM-coated plate and incubated for 1 hour at 30 °C with gentle shaking at 600 rpm. The signal was detected by Sector Imager 2400 (Meso Scale Discovery). The data were further processed to obtain the ratio of detected signal for each sample to that of tocilizumab (assay control).

Capillary isoelectric focusing

cIEF analyses of antibodies were performed with a Maurice system (Protein Simple). Briefly, 8.5 μ L of 0.5 mg/mL concentration of antibody solutions were diluted with 41.5 μ L of cIEF master mix solution containing methyl cellulose, urea, Pharmalyte 5–8 and 8–10.5, arginine, iminodiacetic acid, and pI markers. Samples were focused at 1500 volts for 1 minute, followed by 3000 volts for 6 minutes. The pI of each of the antibodies was analyzed using Compass for iCE software.

Abbreviations

ACE2	Angiotensin-converting enzyme 2
AC-SINS	Affinity-capture self-interaction nanoparticle spectroscopy
ADE	Antibody-dependent Enhancement
AUC	Area under the curve
CDR	Complementary-determining region
CHO	Chinese hamster ovary
CL	Clearance
COVID-19	Coronavirus disease 2019
ECM	Extracellular matrix
Fab	Fragment antigen binding
Fc	Fragment crystallizable
Fc γ R	Fc gamma receptor
FcRn	Neonatal Fc receptor
HEK	Human Embryonic Kidney
HIC	Hydrophobic interaction chromatography
HMW	High molecular weight
IgG	Immunoglobulin G
IVIG	Intravenous immune globulin
mAb	monoclonal antibody
pI	Isoelectric point
PK	Pharmacokinetic
RBD	Receptor binding domain
SARS-CoV-2	Severe acute respiratory syndrome coronavirus 2
SEC	Size-exclusion chromatography
TSA	Thermal shift assay
VOCs	Variants of concern
VOIs	Variants of interest
WT	Wildtype

Acknowledgments

The authors thank all research assistants in Chugai Pharmabody Research Pte. Ltd. for excellent experiment assistance. The authors thank Professor Yee-Joo Tan (Department of Microbiology, NUS; Institute of Molecular and Cell Biology, A*STAR) who kindly provided CHO-ACE2 cells. The authors thank Dr Brendon John Hanson from DSO laboratories for pTT5LnX-CoV-SP plasmid used to generate pseudovirus.

Disclosure statement

No potential conflict of interest was reported by the author(s).

Funding

This work was supported by Chugai Pharmaceutical Co. Ltd. This work was also supported by core research grants provided to the Singapore Immunology Network by the Biomedical Research Council (BMRC) and the A*CCLERATE GAP fund (ACCL/19-GAP064-R20H-I) from the Agency of Science, Technology and Research A*CCLERATE GAP fund ACCL/19-GAP064-R20H-I. Funding to pay the Open Access publication charges for this article was provided by Chugai Pharmaceutical Co. Ltd.

Singapore Immunology Network (SigN) at the Agency of Science, Technology and Research (A*STAR) of Singapore (<https://www.a-star.edu.sg/sign>).

ORCID

Taichi Kuramochi  <http://orcid.org/0000-0001-7242-7124>
 Bei Wang  <http://orcid.org/0000-0002-3112-7341>
 Dan Chen  <http://orcid.org/0000-0002-2790-5606>
 Wen-Hsin Lee  <http://orcid.org/0000-0003-0315-7495>
 Eve Zi Xian Ngoh  <http://orcid.org/0000-0001-5407-0280>
 Cheng-I Wang  <http://orcid.org/0000-0001-9170-2996>
 Hideaki Shimada  <http://orcid.org/0000-0003-4932-1385>

References

- Weinreich DM, Sivapalasingam S, Norton T, Ali S, Gao H, Bhore R, Musser BJ, Soo Y, Rofail D, Im J, et al. REGN-COV2, a Neutralizing Antibody Cocktail, in Outpatients with Covid-19. *N Engl J Med.* 2020;384(3):238–51. doi:10.1056/NEJMoa2035002.
- Piccoli L, Park Y-J, Tortorici MA, Czudnochowski N, Walls AC, Beltramello M, Silacci-Fregni C, Pinto D, Rosen LE, Bowen JE, et al. Mapping Neutralizing and Immunodominant Sites on the SARS-CoV-2 Spike Receptor-Binding Domain by Structure-Guided High-Resolution Serology. *Cell.* 2020;183(4):1024–1042.e1021. doi:10.1016/j.cell.2020.09.037.
- Taylor PC, Adams AC, Hufford MM, de la Torre I, Winthrop K, Gottlieb RL. Neutralizing monoclonal antibodies for treatment of COVID-19. *Nat Rev Immunol.* 2021;21(6):382–93. doi:10.1038/s41577-021-00542-x.
- Polack FP, Thomas SJ, Kitchin N, Absalon J, Gurtman A, Lockhart S, Perez JL, Pérez Marc G, Moreira ED, Zerbini C, et al. Safety and Efficacy of the BNT162b2 mRNA Covid-19 Vaccine. *N Engl J Med.* 2020;383(27):2603–15. doi:10.1056/NEJMoa2034577.
- Baden LR, El Sahly HM, Essink B, Kotloff K, Frey S, Novak R, Diemert D, Spector SA, Rouphael N, Creech CB, et al. Efficacy and Safety of the mRNA-1273 SARS-CoV-2 Vaccine. *N Engl J Med.* 2020;384(5):403–16. doi:10.1056/NEJMoa2035389.
- Planas D, Veyer D, Baidaliuk A, Staropoli I, Guivel-Benhassine F, Rajah MM, Planchais C, Porrot F, Robillard N, Puech J, et al. Reduced sensitivity of SARS-CoV-2 variant Delta to antibody neutralization. *Nature.* 2021;596(7871):276–80. doi:10.1038/s41586-021-03777-9.
- Wang P, Nair MS, Liu L, Iketani S, Luo Y, Guo Y, Wang M, Yu J, Zhang B, Kwong PD, et al. Antibody resistance of SARS-CoV-2 variants B.1.351 and B.1.1.7. *Nature.* 2021;593(7857):130–35.
- Falcone M, Tiseo G, Valoriani B, Barbieri C, Occhineri S, Mazzetti P, Vatteroni ML, Suardi LR, Riccardi N, and Pistello M, et al. Efficacy of Bamlanivimab/Etesevimab and Casirivimab/Imdevimab in Preventing Progression to Severe COVID-19 and Role of Variants of Concern. *Infect Dis Ther.* 2021;10(4):2479–2488.
- Cao Y, Wang J, Jian F, Xiao T, Song W, Yisimayi A, Huang W, Li Q, Wang P, An R, et al. Omicron escapes the majority of existing SARS-CoV-2 neutralizing antibodies. *Nature.* 2021. doi:10.1038/s41586-021-04385-3.
- Asarnow D, Wang B, Lee WH, Hu Y, Huang CW, Faust B, Ng PML, Ngoh EZX, Bohn M, Bulkley D, et al. Structural insight into SARS-CoV-2 neutralizing antibodies and modulation of syncytia. *Cell.* 2021;184(12):3192–3204.e3116. doi:10.1016/j.cell.2021.04.033.
- Wang B, Asarnow D, Lee W-H, Huang C-W, Faust B, Ng PML, Ngoh EZX, Bohn M, Bulkley D, and Pizzorno A, et al. Bivalent binding of a fully human IgG to the SARS-CoV-2 spike proteins reveals mechanisms of potent neutralization. *bioRxiv.* accessed. 2020. Jul. 15. [accessed 2020 Jul 15]. doi:10.1101/2020.07.14.203414.<https://www.biorxiv.org/content/10.1101/2020.07.14.203414v1.full>
- Maeda A, Iwayanagi Y, Haraya K, Tachibana T, Nakamura G, Nambu T, Esaki K, Hattori K, Igawa T. Identification of human IgG1 variant with enhanced FcRn binding and without increased binding to rheumatoid factor autoantibody. *mAbs.* 2017;9(5):844–53. doi:10.1080/19420862.2017.1314873.
- Berteau C, Filipe-Santos O, Wang T, Roja HE, Granger C, Schwarzenbach F. Evaluation of the impact of viscosity, injection volume, and injection flow rate on subcutaneous injection tolerance. *Med Devices (Auckl).* 2015;8:473–84. doi:10.2147/MDER.S91019.
- Igawa T, Tsunoda H, Tachibana T, Maeda A, Mimoto F, Moriyama C, Nanami M, Sekimori Y, Nabuchi Y, Aso Y, et al. Reduced elimination of IgG antibodies by engineering the variable region. *Protein Eng Des Sel.* 2010;23(5):385–92. doi:10.1093/protein/gzq009.
- Zhang Y, Wu L, Gupta P, Desai AA, Smith MD, Rabia LA, Ludwig SD, Tessier PM. Physicochemical Rules for Identifying Monoclonal Antibodies with Drug-like Specificity. *Mol Pharm.* 2020;17(7):2555–69. doi:10.1021/acs.molpharmaceut.0c00257.
- O'Brien MP, Forleo-Neto E, Musser BJ, Isa F, Chan K-C, Sarkar N, Bar KJ, Barnabas RV, Barouch DH, Cohen MS, et al. Subcutaneous REGEN-COV Antibody Combination to Prevent Covid-19. *N Engl J Med.* 2021;385(13):1184–95. doi:10.1056/NEJMoa2109682.
- Bauer J, Mathias S, Kube S, Otte K, Garidel P, Gamer M, Blech M, Fischer S, Karow-Zwick AR. Rational optimization of a monoclonal antibody improves the aggregation propensity and enhances the CMC properties along the entire pharmaceutical process chain. *mAbs.* 2020;12(1):1. doi:10.1080/19420862.2020.1787121.
- Muecksch F, Weisblum Y, Barnes CO, Schmidt F, Schaefer-Babajew D, Wang Z, Lorenzi JC C, Ai F, AT D, KE H-T, et al. Affinity maturation of SARS-CoV-2 neutralizing antibodies confers potency, breadth, and resilience to viral escape mutations. *Immunity.* 2021;54(8):1853–1868.e1857. doi:10.1016/j.immuni.2021.07.008.
- Sokal A, Barba-Spaeth G, Fernández I, Broketa M, Azzaoui I, de La Selle A, Vandenberghe A, Fourati S, Roeser A, Meola A, et al. mRNA vaccination of naive and COVID-19-recovered individuals elicits potent memory B cells that recognize SARS-CoV-2 variants. *Immunity.* 2021;54(12):2893–2907.e2895. doi:10.1016/j.immuni.2021.09.011.
- Starr TN, Greaney AJ, Addetia A, Hannon WW, Choudhary MC, Dingens AS, Li JZ, Bloom JD. Prospective mapping of viral mutations that escape antibodies used to treat COVID-19. *Science.* 2021;371(6531):850–54. doi:10.1126/science.abf9302.
- Groves MAT, Amanuel L, Campbell JI, Rees DG, Sridharan S, Finch DK, Lowe DC, Vaughan TJ. Antibody VH and VL recombination using phage and ribosome display technologies reveals distinct structural routes to affinity improvements with VH-VL interface residues providing important structural diversity. *mAbs.* 2014;6(1):236–45. doi:10.4161/mabs.27261.
- Lip K-M, Shen S, Yang X, Keng C-T, Zhang A, Oh H-LJ, Li Z-H, Hwang L-A, Chou C-F, Fielding BC, et al. Monoclonal Antibodies Targeting the HR2 Domain and the Region Immediately Upstream of the HR2 of the S Protein Neutralize In Vitro Infection of Severe Acute Respiratory Syndrome Coronavirus. *Journal of Virology.* 2006;80(2):941–50. doi:10.1128/JVI.80.2.941-950.2006.